




Terahertz laser diode using field emitter arraysWeihao Liu **College of Electronic and Information Engineering, Nanjing University of Aeronautics and Astronautics, Nanjing, Jiangsu 211106, China*Yucheng Liu , Qika Jia, and Baogen Sun*National Synchrotron Radiation Laboratory, University of Science and Technology of China, Hefei, Anhui 230029, China*

Jun Chen

School of Electronics and Information Technology, Sun Yat-Sen University, Guangzhou 510275, China (Received 3 March 2020; revised 17 December 2020; accepted 23 December 2020; published 7 January 2021)

High-power and broad-tunable terahertz wave generating source on chip, which has broad application prospects, remains an unachieved goal of researchers after decades of pursuing. Here, we propose a concept of terahertz laser diode, which is a dc-biased self-excited microelectronic laser oscillator using collectively modulated free electrons emitted by field-emitter-arrays as the active medium and using an inherent Fabry-Pérot interferometer formed by port reflections as the frequency selector. It is sub-millimeter to centimeter in size and can generate continuous-wave coherent terahertz radiation with several watts of power per square millimeter. Its frequency can be tuned to cover a wide terahertz band by changing the cathode-to-anode distance and the bias voltage. It has the potential to outperform the conventional free-electron or solid-state terahertz devices in terms of portability, tunability, and output power, signifying a promising class of tunable and high-power terahertz source on chip.

DOI: [10.1103/PhysRevB.103.035109](https://doi.org/10.1103/PhysRevB.103.035109)**I. INTRODUCTION**

The terahertz electromagnetic wave is believed to have broad application prospects in diverse scientific and technological fields [1–4]. However, the lack of desirable terahertz generating source has still been the primary bottleneck that restricts the advancements of terahertz technologies [5,6]. Restricted by the band-gap property of active material, the frequency of conventional lasers can hardly go down to the terahertz region [7]. The quantum cascaded laser can generate terahertz emission only under extremely low-temperature circumstances [8,9]. High-power, broad-tunable, and working-in-room-temperature terahertz laser on chip has always been a pursuit of researchers.

Extending the frequencies of conventional vacuum electron devices (VEDs) [10,11] and solid-state electron devices (SEDs) [12] from the subterahertz region is another option for the terahertz wave generation. The conventional VEDs, using free-electron beams to induce and amplify microwave fields, are known for high power and high efficiency [13]. Yet, they have the innate disadvantages of high cost, high energy-consumption, and a short lifetime. Also, in the terahertz region, they encounter the challenges of manufacturing tiny-size structures [14,15] and of producing electron beams with extremely high current densities [16,17]. SEDs overcome the weaknesses of VEDs: they have low cost, low power-consumption, and a long lifetime. In addition, they can easily

be fabricated and be integrated on chip. Unfortunately, SEDs are not capable of generating terahertz radiation due to the restriction of electron mobility in solid-state materials. In practice, high-order frequency multipliers have to be used in the terahertz region [18–20], which increases the cost and decreases the output power in consequence.

The recently developed vacuum microelectronic devices (VMDs), which are micrometerscale versions of VEDs using advanced microfabrication techniques and a field-emission cold cathode, can promisingly combine both the advantages of high-efficiency and miniaturization [21–25]. Yet still, they cannot generate or amplify the terahertz radiation efficiently since the operating frequency is largely determined by the transverse dimension of the electrode, which has to be far less than $1\ \mu\text{m}$ in the terahertz region [26,27], greatly restricting the lifetime and power capacity of the device.

In the present paper, aiming to develop a high-power terahertz source on chip, we propose the concept of a free-electron terahertz laser diode (TLD), which is a modified VMD with an alternative mechanism. It can generate coherent continuous-wave terahertz radiation with several milliwatts of power from a millimeter on-chip device, which outperforms the conventional free-electron or solid-state terahertz devices and lasers in terms of portability, tunability, and output power, signifying a unique and promising class of tunable and high-power terahertz source on chip.

II. MODEL DESCRIPTION

The schematic diagram of the proposed TLD is illustrated in Fig. 1. It is a dc-biased microelectronic biplanar-diode

*liuwhao@nuaa.edu.cn

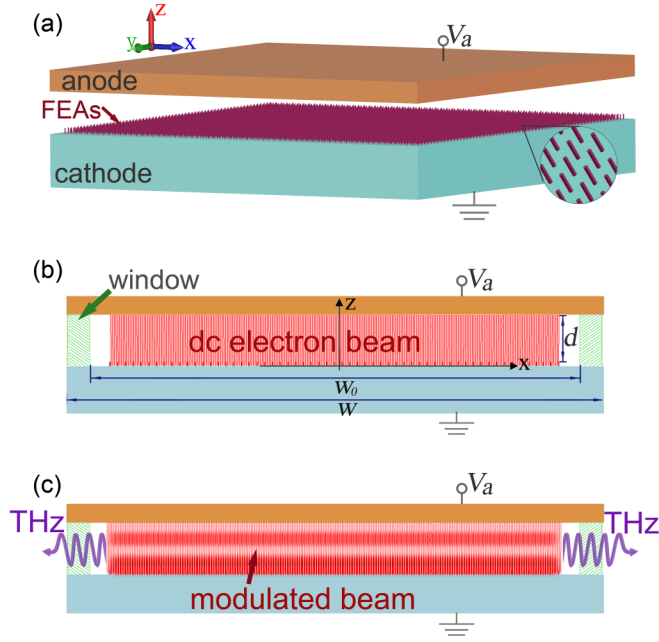


FIG. 1. (a) Schematic model of the proposed TLD without output windows. (b) The two-dimensional (2D) model of TLD with a dc electron beam. (c) The 2D model of TLD with a modulated beam and THz emission.

using a cold cathode with field emitter arrays (FEAs). The two parallel electrodes are upheld by two dielectric pillars at both ends, which also work as the output windows. The operating mechanism of the TLD is essentially different from that of the conventional VEDs, SEDs, and VMDs, and it can be briefly stated as follows. Driven by the static electric field in the diode, the FEAs emit a dc electron beam, see Fig. 1(b), which induces time-harmonic fields (THFs) in the terahertz region. These THFs then modulate the electron beam emission in return; namely, the electron beam is premodulated initially from the cathode. The premodulated electron beam then interacts with the THFs via gaining or losing its kinetic energy. In a certain spectral range, the electron beam gains net energy from the THFs, which will decay quickly, while in other spectral ranges, it transfers net kinetic energy to the THFs, which will be amplified. These amplified THFs will further modulate the beam emission and then be further amplified; namely, the positive feedback loop is achieved. The THFs will be reflected back and forth at both ends of the diode due to the abrupt changes of boundaries [28], forming certain resonant modes—the operation modes—in the diode, which is in physics similar to light waves in a Fabry-Pérot (FP) interferometer of a conventional laser. A portion of electromagnetic energy will be output through the windows as shown in Fig. 1(c), generating a monochromatic (coherent) continuous-wave terahertz radiation. Therefore, the TLD is in essence a self-amplified self-excited oscillator powered by the collectively modulated free-electron beam, which operates as an effectively active medium. It is remarkably different from the conventional laser, which resorts to the bound-electron's transition between different energy levels of the active medium. The operating frequency of the conventional laser is determined and restricted by the band-gap structure

of the active medium. In contrast, the frequency of the TLD depends on the structural parameters and on the bias voltage, which can be readily tuned in practice.

III. ANALYTICAL FORMULATION

In the following, we perform analytical explorations and simulations of a TLD. As indicated in Sec. II, a key component of the TLD is the FEA, which has been experiencing a rapid development thanks to its broad application prospects [29]. The emitted electron beam current density (J_s) from FEAs can be expressed by the simplified Fowler-Nordheim (F-N) formula [30]:

$$J_s = aE_s^2 \exp\left(\frac{-b}{E_s}\right), \quad (1)$$

in which a and b are the field-emission coefficients and E_s is the electric field on the cathode surface. In practice, the FEAs are composed of a large amount of nanoscale emitters (carbon nanotubes [31,32] or ZnO nanowires [33–35], for example) as depicted in Fig. 1(a), such that the electric fields at the emitting tips are tremendously enhanced. Since the spacings between adjacent nanotips are much less than the operating wavelength as well as the transverse size of the TLD, the FEA can be approximately treated as a planar electrode with scaled field-emission parameters.

When the THF is excited within the diode, E_s can be expressed as $E_s = E_{s0} + E_{s1} \sin(\omega t + \varphi_0)$, in which the first and the second terms denote the dc field and the THF, respectively. ω is the angular frequency of the THF and φ_0 is the initial phase of the THF at the cathode surface experienced by the emitted electrons. Substituting it into Eq. (1) and then using the Fourier expansion, one can get that the emitted beam current density also consists of the dc field and THF components: $J_s = J_{s0} + J_{s1} \sin(\omega t + \varphi_0)$, in which we only consider the dominant part and ignore high harmonic ones [28]. In other words, the emitted beam current has been modulated from the beginning. This initially modulated electron beam interacts with the THF via gaining or losing kinetic energy as it moves from the cathode to the anode. The power per unit area received by the electron beam from the THF can be expressed as

$$P(\varphi_0) = \int_0^d [J_{s0} + J_{s1} \sin \varphi_0] \times \left[E_0(z) + E_1 \sin\left(\int \frac{\omega dz}{v(z)} + \varphi_0\right) \right] dz. \quad (2)$$

Here we assume that the phase and the amplitude of the THF do not change with z ($E_1 = E_{s1}$), which is reasonable since the width between the cathode and the anode is much less than the wavelength of the THF ($d \ll \lambda$). Note that each electron will experience a changing phase of the THF as it moves from the cathode to the anode. We call this phase variation the transition phase, which is expressed by $\Delta\varphi = \omega\Delta t = \omega \int \frac{dz}{v(z)}$ as given above. The average power per unit area received by the electron beam from the THF within a whole oscillating period can then be obtained by

$$P_t = \int_0^{2\pi} P(\varphi_0) d\varphi_0. \quad (3)$$

We note that the integral kernel of Eq. (2) is composed of four parts. The first one is the dc component and is always positive, indicating that the dc electron beam will be accelerated by the dc electric field. The second and third parts with the linear term of the oscillating component $\sin \varphi_0$, respectively, denote the work done by the dc field on the modulated electron beam and the work done by the THF on the dc beam. They will vanish after the integration in Eq. (3); in other words, the THF cannot be amplified by a dc electron beam. The fourth part with the quadratic term of $\sin \varphi_0$ denotes the work done by the THF on the modulated component of the electron beam. It can be positive or negative and is what we mainly deal with. If it is positive, the net energy will be transferred from the THF to the electron beam; otherwise, the THF will gain net energy and will be amplified, which is exactly the essence of a TLD.

To work out Eq. (2), we resort to the following Poisson equation,

$$\frac{\partial^2 \Phi(z)}{\partial z^2} = -\frac{\rho(z)}{\epsilon_0}, \quad (4)$$

by which the space charge effect of the electron beam is taken into consideration, and the energy conservation equation,

$$2\eta\Phi(z) = v^2(z) - v^2(0). \quad (5)$$

Here Φ is the electric potential, ρ is the charge density, ϵ_0 is the permittivity of the vacuum, η is the charge-to-mass ratio of the electrons, and $v(0)$ is the initial velocity of the field-emitted electrons, which has been extensively investigated in previous literature [36]. To solve these equations, the electron velocity, the charge density, and the electric potential also have to be decomposed into dc parts and time-harmonic ones: $v(z) = v_0(z) + v_1(z) \sin(\omega\Delta_t + \varphi_0)$, $\rho(z) = \rho_0(z) + \rho_1(z) \sin(\omega\Delta_t + \varphi_0)$, and $\Phi(z) = \Phi_0(z) + \Phi_1(z) \sin(\omega t + \varphi_0)$. Substituting them into Eqs. (4) and (5), we can get two sets of equations, dealing with the dc field and the THF, respectively [28]. Both of them have to be solved by using a numerical method.

The amplified THF will propagate in the transverse (x) direction of the diode, part of which will be output through the dielectric windows, balancing the energy of the THF in the diode. Besides, since the cathode-to-anode distance d is much less than the operating wavelength ($d \ll \lambda$) and the transverse size (w) of the diode ($d \ll w$), a large portion of the THF will be reflected at the apertures due to the abrupt change of boundaries, forming a series of resonant modes in the diode. Under this condition, the two apertures can be approximated as perfect-magnetic-conductor walls [37]. Since the diode is structurally symmetric in the x direction, the resonant modes consist of even modes and odd ones, respectively, with electric fields being symmetrically and antisymmetrically distributed along the center line $x = 0$. In the practice of TLD, we find that only the even modes can effectively interact with the electron beam and can be amplified. In other words, the even FP modes are the operation modes of TLD. Using the mode-matching method, the dispersion equation of the even modes can be obtained [28] as

$$\frac{e^{j\sqrt{\epsilon_r}k_0w} e^{-jk_0\sqrt{\epsilon_r}w_0} - e^{-jk_0w_0}}{e^{j\sqrt{\epsilon_r}k_0w} e^{-j(\sqrt{\epsilon_r}+1)k_0w_0} - 1} = \frac{1 - \sqrt{\epsilon_r}}{1 + \sqrt{\epsilon_r}}, \quad (6)$$

in which $k_0 = \omega/c$ is the wave number *in vacuo*, c is the speed of light *in vacuo*, and ϵ_r is the dielectric constant of the windows. w and w_0 are the structure parameters of the diode shown in Fig. 1. By numerically solving Eq. (6), the field properties and frequencies of the resonant modes in the diode can be obtained.

IV. NUMERICAL CALCULATION, SIMULATION, AND DISCUSSION

In this section, we carry out calculations and simulations on the proposed TLD. The simulations are performed by using fully electromagnetic particle-in-cell codes [38,39]. Both the cathode and the anode are set to be copper (lossy metal) with a conductivity of 10^7 S/m. The field-emission parameters are set to $a = 3.6 \times 10^{-9}$ A/m² and $b = 4 \times 10^6$ V/m, which are obtained by fitting the emission curves experimentally obtained in the previous literature [31,32]. The cathode-to-anode gap is set to be $d = 10$ μ m and the transverse parameters of the diode are set to $w = 0.4$ mm and $w_0 = 0.38$ mm (the thickness of the dielectric window is 20 μ m). The dielectric constant of the output window is $\epsilon_r = 3.8$ and the bias voltage is $V_a = 1.5$ kV. The simulated electric field at the surface of the cathode and the emitted beam current density, together with their frequency spectra, are illustrated in Figs. 2(a) and 2(b), respectively. We can see that the field within the diode and the emitted current are both composed of the dc field and the THF (with a frequency of 0.89 THz) as predicted. Figure 2(c) illustrates the simulated THF (E_z) and the charge density (ρ) of the electron beam in the time domain detected at different longitudinal positions (from $z = 0.05d$ to $z = 0.9d$). As predicted, the amplitude and the phase of the THF almost do not change in the z direction, and yet those of the charge density ρ change obviously with z (there exists a phase delay), which is because the electron velocity is much less than the speed of light and it needs a certain time duration for the electrons to transport the oscillating signal. We note that ρ and E are in phase (oscillating synchronously) at the cathode surface ($z = 0.05d$) and the phase deviation increases gradually with z , indicating that the electrons experience different phases of the THF as they move from the cathode to the anode, agreeing with our prediction. Also, we find that the charge density is initially modulated, with the bunch centers located at the peak accelerating points ($\varphi = 2n\pi + \pi/2$), and yet these bunch centers slip to the decelerating regions as they transit to the anode. Notably, they slip faster at the beginning than at the end, namely, the electron bunches enter into the deceleration regions quickly while leaving slowly (they stay in the decelerating regions from $z = 0.2d$ to the end as shown in the figure), such that they will experience more deceleration than acceleration, transferring net energy to and amplifying the THF. It can be understood that the electron velocity $v(z)$ increases gradually as the electrons move from the cathode to the anode, resulting in the rate of the phase-slippage, expressed by $d\varphi = \omega \frac{dz}{v(z)}$ according to Eq. (2), decreasing with z . Besides that, we note that the bunch size decreases gradually with z , indicating that the charge density of the premodulated beam is further modulated as the electrons move to the anode, which is due to the initial velocity modulation of the electron beam emitted from FEAs.

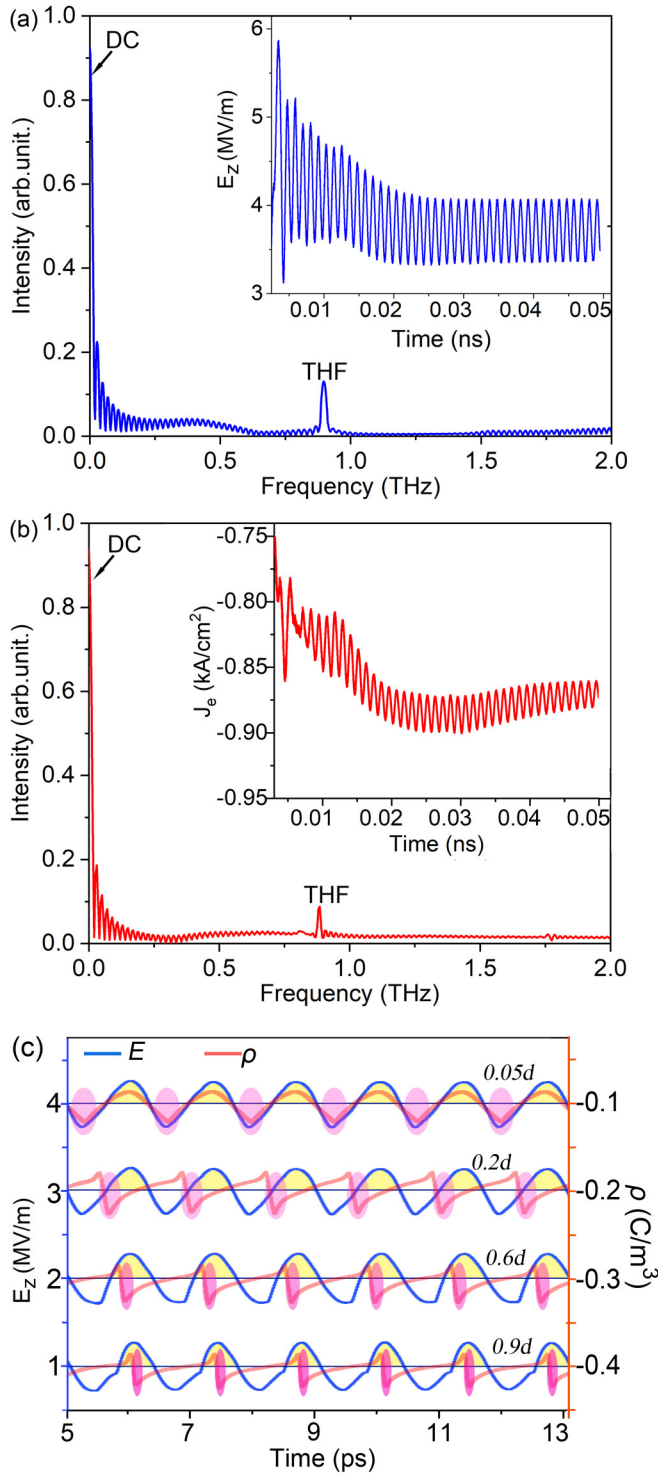


FIG. 2. Simulated electric field at the surface of the cathode (a) and the emitted beam current density (b), together with their frequency spectra. (c) Simulated THF E (in blue) and charge density ρ (in pink) in the time domain detected at different longitudinal positions (from $z = 0.05d$ to $z = 0.9d$). ρ is negative since the electron carries a negative charge. The yellow regions denote the decelerating regions and the purple ellipses approximately locate the electron bunches.

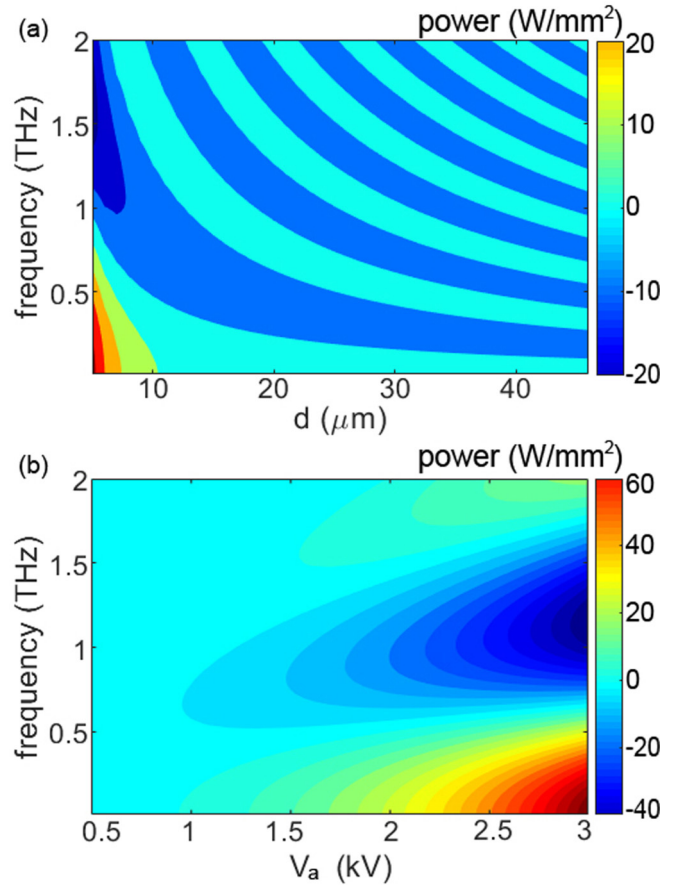


FIG. 3. (a) The calculated power as a function of cathode-anode distance d and frequency. Here the bias voltage is $V_a = 1.5$ kV. (b) The calculated power as a function of bias voltage V_a and frequency. Here $d = 10$ μm . The negative power regions denote the possible operation regions.

Figure 3(a) illustrates the calculated power received by the electron beam from the THF as a function of cathode-to-anode width d and of frequency (here the bias voltage V_a is 1.5 kV). We note that it varies from positive to negative alternately, indicating that the electrons will gain or lose net energy depending on operating parameters and on the frequency. The negative-power regions denote the possible operation regions, in which THFs receive net energy from the electron beam and are amplified. These operation regions define the achievable spectral range of the TLD. In each operation region, the achievable frequency generally decreases as d increases. For the lowest operation region, which is generally the dominant region in practice, the achievable operating frequency ranges from 0.2 to 2 THz as d changes from 6 to 40 μm . The calculated power as a function of the bias voltage V_a and of the frequency is presented in Fig. 3(b) (here $d = 10$ μm), which shows that the achievable frequency increases as V_a increases, and it ranges from 0.5 to 1.5 THz as V_a changes from 0.5 to 3 kV. These dependencies of the frequency on V_a and d can be explained as follows. As indicated in Fig. 2(c), the time period T_e of the THF is essentially determined by the transition time duration of the electrons (especially at the bunch centers) in

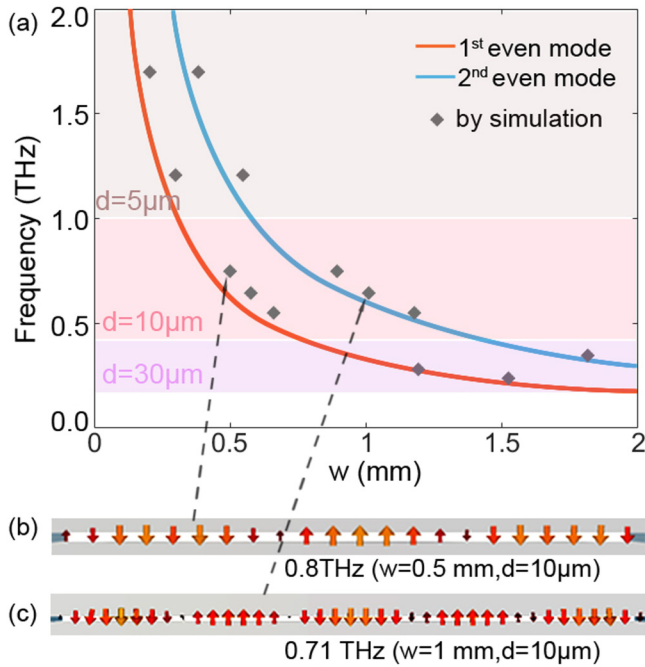


FIG. 4. (a) Calculated (lines) and simulated (dots) operating frequencies of the TLD as a function of w . Here two FP modes with $n = 1$ and $n = 2$ are shown. (b) Simulated electric field distribution at 0.8 THz for $d = 10 \mu\text{m}$ and $w = 0.5 \mu\text{m}$. (c) Simulated electric field distribution at 0.71 THz for $d = 10 \mu\text{m}$ and $w = 1 \mu\text{m}$.

the diode Δ_t . A high operating frequency ($f = 1/T_e$) means a small Δ_t , which can be achieved by a large V_a or a small d .

While V_a and d define the achievable frequency range of the TLD, the exact operating frequency is determined by the FP resonant modes in the diode and can be tuned by changing w , w_0 , or ϵ_r according to Eq. (7). Naturally, the tunable range should be located in the operation regions of the TLD. Figure 4(a) shows the calculated and simulated operating frequency of the TLD as a function of w while the thickness of the dielectric window is kept to $20 \mu\text{m}$. In calculations, the lowest two even FP modes are presented. We note that the simulated results agree well with the calculated ones. By choosing three values of d , 5, 10, and $30 \mu\text{m}$, the operating frequency of the TLD can be tuned from 0.2 to 2 THz by varying w . Figures 4(b) and 4(c) illustrate the simulated electric field distributions at two operating frequencies (0.8 and 0.71 THz) for the diode with two sets of structure parameters. They respectively represent the first and the second even FP modes as predicted.

The calculated and simulated output power and efficiency of the TLD as functions of V_a and d are presented in Fig. 5. Figure 5(a) shows that the power increases with V_a and decreases with d . It can reach several to tens of watts per square millimeter at ~ 1 THz, which is higher than most of the available terahertz sources [5]. Figure 5(b) shows that the efficiency (the output power divided by the electron beam power) increases as d increases or as V_a decreases. It can be understood that a larger d or a smaller V_a leads to a larger transition time, such that electrons can interact with the THF more sufficiently. In addition, the emitted beam current,

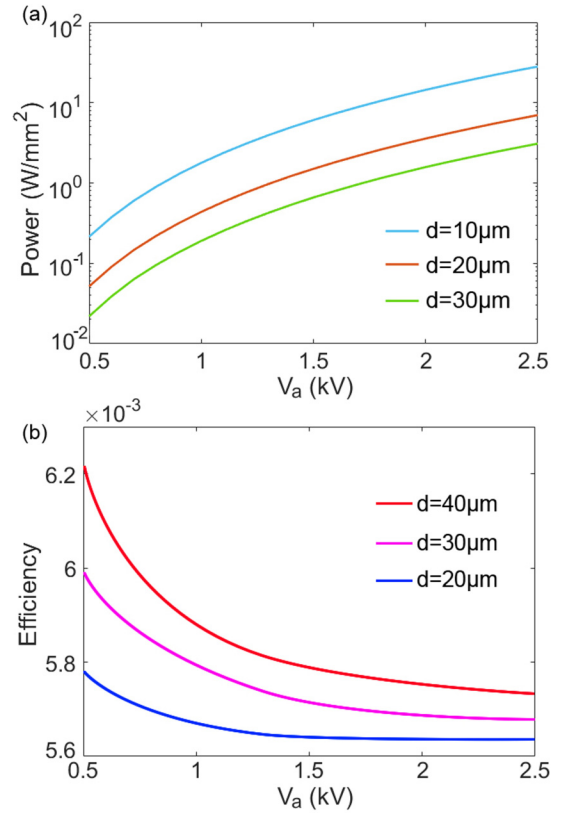


FIG. 5. Calculated power (a) and efficiency (b) of the TLD as functions of d and V_a .

together with the input power of the electron beam, decreases quickly as d increases or as V_a decreases according to the F-N formula, which enhances the power efficiency in effect. The efficiency of the present TLD model is at the level of 10^{-3} . We find that this efficiency can be improved by using appropriate techniques, which will be further discussed in the future.

V. CONCLUSION

In conclusion, we proposed and investigated a free-electron terahertz laser diode, which is essentially a self-amplified self-excited electromagnetic emission from a collectively modulated free-electron beam. Net energy is transferred from the premodulated electron beam to the terahertz wave due to the phase slippage of the electron bunches as they transit from the cathode to the anode. The electron transition time determines the achievable spectral range of the terahertz laser diode. The monochromatic emission is achieved via a built-in Fabry-Pérot resonator formed by two dielectric windows. This proposed terahertz laser diode is sub-millimeter to centimeter in size and can be easily integrated on chip. Its average power can reach several to tens of watts per square millimeter by using readily available structures and operation parameters. It affords a promising way of developing high-power and broad-tunable continuous-wave terahertz sources on chip.

ACKNOWLEDGMENTS

This work was supported by the Natural Science Foundation of China (Grants No. U1632150, No. 61471332, and No. 11675178).

- [1] M. Tonouchi, Cutting-edge terahertz technology, *Nat. Photonics* **1**, 97 (2007).
- [2] L. A. Downes, A. R. MacKellar, D. J. Whiting, C. Bourgenot, C. S. Adams, and K. J. Weatherill, Full-Field Terahertz Imaging at KiloHertz Frame Rates Using Atomic Vapor, *Phys. Rev. X* **10**, 011027 (2020).
- [3] R. Kowerdziej, M. Olifierczuk, J. Parka, and J. Wróbel, Terahertz characterization of tunable metamaterial based on electrically controlled nematic liquid crystal, *Appl. Phys. Lett.* **105**, 022908 (2014).
- [4] N. Laman, M. Bieler, and H. M. van Driel, Ultrafast shift and injection currents observed in wurtzite semiconductors via emitted terahertz radiation, *J. Appl. Phys.* **98**, 103507 (2005).
- [5] S. S. Dhillon, M. S. Vitiello, E. H. Linfeld, A. G. Davies, M. C Hoffmann, J. Booske, C. Paoloni, M. Gensch, P. Weightman, G. P. Williams *et al.*, The 2017 terahertz science and technology roadmap, *J. Phys. D: Appl. Phys.* **50**, 043001 (2017).
- [6] F. Friederich, W. von Spiegel, M. Bauer, F. Meng, M. D. Thomson, S. Boppel, A. Lisauskas, B. Hils, V. Krozer, A. Keil, T. Löffler, R. Henneberger, A. K. Huhn, G. Spickermann, P. H. Bolivar, and H. G. Roskos, THz active imaging systems with real-time capabilities, *IEEE Trans. Terahertz Sci. Technol.* **1**, 183 (2011).
- [7] Karl F. Renk, *Basics of Laser Physics*, (Springer-Verlag, Berlin, 2012).
- [8] R. Eichholz, H. Richter, M. Wienold, L. Schrottke, R. Hey, H. T. Grahn, and H.-W. Hübers, Frequency modulation spectroscopy with a THz quantum-cascade laser, *Opt. Express* **21**, 32199 (2013).
- [9] B. S. Williams, S. Kumar, Q. Hu, and J. L. Reno, Operation of terahertz quantum-cascade lasers at 164 K in pulsed mode and at 117 K in continuous-wave mode, *Opt. Express* **13**, 3331 (2005).
- [10] P. H. Siegel, Terahertz technology, *IEEE Trans. Microwave Theory Tech.* **50**, 910 (2002).
- [11] M. A. Basten, J. C. Tucek, D. A. Gallagher, K. E. Kreischer, R. Mihailovich, A 0.85 THz vacuum-based power amplifier, in *Proceedings of the 2012 IEEE Thirteenth International Vacuum Electronics Conference (IVEC)* (IEEE, New York, 2012), pp. 39–40.
- [12] A. Maestrini, I. Mehdi, J. V. Siles, J. S. Ward, R. Lin, B. Thomas, C. Lee, J. Gill, G. Chattopadhyay, E. Schlecht, J. Pearson, and P. Siegel, Design and characterization of a room temperature all-solid-state electronic source tunable from 2.48 to 2.75 THz, *IEEE Trans. Terahertz Sci. Technol.* **2**, 177 (2012).
- [13] J. H. Booske, R. J. Dobbs, C. D. Joye, C. L. Kory, G. R. Neil, G.-S. Park, J. Park, and R. J. Temkin, Vacuum electronic high power terahertz sources, *IEEE Trans. Terahertz Sci. Technol.* **1**, 54 (2011).
- [14] Y.-M. Shin, L. R. Barnett, and N. C. Luhmann, Jr., MEMS-fabricated microvacuum electron devices for terahertz (THz) applications, in *Proceedings of the International Conference on Infrared, Millimeter, and Terahertz Waves (IRMMW-THz)*, 2008 (IEEE, Pasadena, CA, 2008), Paper 1.1591.
- [15] M. Mineo and C. Paoloni, Corrugated rectangular waveguide tunable backward wave oscillator for terahertz applications, *IEEE Trans. Electron Devices* **57**, 1481 (2010).
- [16] D. H. Shin, K. N. Yun, J. S. Han, C. J. Lee, S.-G. Jeon, and D. Shin, Sheet electron beam from line-shape carbon nanotube field emitters, in *Proceedings of the 28th International Vacuum Nanoelectronics Conference (IVNC)*, 2015 (IEEE, Guangzhou, China, 2015), pp. 216–217.
- [17] W. He, L. Zhang, D. Bowes, H. Yin, K. Ronald, A. D. R. Phelps, and A. W. Cross, Generation of broadband terahertz radiation using a backward wave oscillator and pseudospark-sourced electron beam, *Appl. Phys. Lett.* **107**, 133501 (2015).
- [18] J. V. Siles, K. B. Cooper, C. Lee, R. H. Lin, G. Chattopadhyay, and I. Mehdi, A new generation of room-temperature frequency-multiplied sources with up to 10× higher output power in the 160-GHz-1.6-THz range, *IEEE Trans. Terahertz Sci. Technol.* **8**, 596 (2018).
- [19] R. Dahlback, J. Vukusic, R. M. Weikle, and J. Stake, A tunable 240–290 GHz waveguide enclosed 2-D grid HBV frequency tripler, *IEEE Trans. Terahertz Sci. Technol.* **6**, 503 (2016).
- [20] S. H. Choi, M. Urteaga, and M. Kim, 600 GHz InP HBT frequency multiplier, *Electron. Lett.* **51**, 1928 (2015).
- [21] J.-W. Han, D.-I. Moon, and M. Meyyappan, Nanoscale vacuum channel transistor, *Nano Lett.* **17**, 2146 (2017).
- [22] S. Nirantar, T. Ahmed, G. Ren, P. Gutruf, C. Xu, M. Bhaskaran, S. Walia, and S. Sriram, Metal-air transistors: Semiconductor-free field-emission air-channel nanoelectronics, *Nano Lett.* **18**, 7478 (2018).
- [23] I. Brodie and P. R. Schwoebel, Vacuum microelectronic devices, *Proc. IEEE* **82**, 1006 (1994).
- [24] S. B. Fairchild, P. Zhang, J. Park, T. C. Back, D. Marincel, Z. Huang, and M. Pasquali, Carbon nanotube fiber field emission array cathodes, *IEEE Trans. Plasma Sci.* **47**, 2032 (2019).
- [25] C. X. Xu, X. W. Sun, and B. J. Chen, Field emission from gallium-doped zinc oxide nanofiber array, *Appl. Phys. Lett.* **84**, 154 (2004).
- [26] J.-W. Han, J. S. Oh, and M. Meyyappan, Vacuum nanoelectronics: Back to the future?—Gate insulated nanoscale vacuum channel transistor, *Appl. Phys. Lett.* **100**, 213505 (2012).
- [27] C. Bower, W. Zhu, D. Shalom, D. Lopez, L. H. Chen, P. L. Gammel, and S. Jin, On-chip vacuum microtriode using carbon nanotube field emitters, *Appl. Phys. Lett.* **80**, 3820 (2002).
- [28] See Supplemental Material at <http://link.aps.org/supplemental/10.1103/PhysRevB.103.035109> for the detailed analytical derivations.
- [29] C. A. Spindt, C. E. Holland, A. Rosengreen, and I. Brodie, Field-emitter arrays for vacuum microelectronics, *IEEE Trans. Electron Devices* **38**, 2355 (1991).
- [30] R. H. Fowler and L. W. Nordheim, Electron emission in intense electric fields, *Proc. R. Soc. London, Ser. A* **119**, 173 (1928).
- [31] J.-W. Kim, J.-W. Jeong, J.-T. Kang, S. Choi, S. Ahn, and Y.-H. Song, Highly reliable field electron emitters produced from reproducible damage-free carbon nanotube composite pastes with optimal inorganic fillers, *Nanotechnology* **25**, 065201 (2014).
- [32] Y. Sun, K. N. Yun, G. Leti, S. H. Lee, Y.-H. Song, and C. J. Lee, High-performance field emission of carbon nanotube paste emitters fabricated using graphite nanopowder filler, *Nanotechnology* **28**, 065201 (2017).
- [33] L. Wang, Y. Zhao, K. Zheng, J. She, S. Deng, N. Xu, and J. Chen, Fabrication of large-area ZnO nanowire field emitter arrays by thermal oxidation for high-current application, *Appl. Surf. Sci.* **484**, 966 (2019).
- [34] J. Chen, Y. Y. Dai, J. Luo, Z. L. Li, S. Z. Deng, J. C. She, and N. S. Xu, Field emission display device structure based on double-gate driving principle for

- achieving high brightness using a variety of field emission nanoemitters, *Appl. Phys. Lett.* **90**, 253105 (2007).
- [35] W. Zhu, Y. Zhang, N. Xu, Y. Tan, R. Zhan, Y. Shen, Z. Xu, X. Bai, J. Chen, J. She, and S. Deng, Epitaxial growth of multiwall carbon nanotube from stainless steel substrate and effect on electrical conduction and field emission, *Nanotechnology* **28**, 305704 (2017).
- [36] J. W. Gadzuk and E. W. Plummer, Field emission energy distribution (FEED), *Rev. Mod. Phys.* **45**, 487 (1973).
- [37] K. Zhang and D. Li, *Electromagnetic Theory in Microwave and Optoelectronics* (Springer-Verlag, Berlin, 2008).
- [38] J. Zhou, D. Liu, C. Liao, and Z. Li, CHIPIC: An efficient code for electromagnetic PIC modeling and simulation, *IEEE Trans. Plasma Sci.* **37**, 2002 (2009).
- [39] CST Corporation, CST PS Tutorials, <http://www.cstchina.cn/>.